INFN_E/GEM4FUSION: GEM AND TIMEPIX BASED DIAGNOSTICS FOR MAGNETIC CONFINEMENT FUSION AND LASER PRODUCED PLASMAS

G. Claps[1,2] (Resp.), V. De Leo[1,2] (Ass.), A. Tamburrino[1,3] (Ass.),
F. Cordella[1,2] (Ass.), D. Pacella[1,2] (Ass.)

1 - INFN – Laboratori Nazionali di Frascati, via E. Fermi 54, 00044 Frascati, Italy
2 - ENEA NUC Department, C. R. Frascati, via E. Fermi 45, 00044 Frascati, Italy
3 - CREF – Centro Ricerche Enrico Fermi, Via Panisperna 89a, 00184 Roma, Italy

Collaborations: CERN-European Organization for Nuclear Research (Switzerland), CNR-ISTP (Milano), Università Milano Bicocca, Université de Bordeaux (France)

1 Introduction

Our research activity was born from a collaboration between ENEA and INFN in Frascati with the main objective of carrying out X-ray and neutron diagnostics of interest in the field of magnetic and inertial confinement nuclear fusion. In particular, most of the scientific program in recent years has included realization and characterization of new 10×10 cm^2 GEM detectors with GEMINI front-end electronics for X-ray imaging and spectroscopy in magnetic confinement fusion and X-ray spectrum measurements on Laser Produced Plasmas (LPP) experiments. In addition, some of the work has been dedicated to the characterization of solid state Timepix-based detectors for the measurements of gamma and neutrons, particularly a new diamond detector based on Timepix3 for fast neutron detection not only on Tokamaks, but also in LPP experiments. All this work is supported by Monte Carlo simulation studies to optimize the new diagnostic systems, in particular, much of the work has been devoted to the evaluation of electronic shielding in high-flux radiation environments. In fact, the development of the new remote front-end electronics arises from the need to protect electronics in high neutron flux environments, as expected on modern fusion reactors like the ITER tokamak. In this last year, our work has been focused on two main research lines: the finalization of the new head-on 10×10 GEM detector with remote electronics, based on 64D GEMINI readout, and the characterization of the side-on 10×10 GEM detector to hard-X rays. In paragraphs 4 and 5, a brief overview of the recent activities on LPPs experiments will also be provided. Further details regarding Timepix-based detectors that are also of interest in the framework of the INFN-E project can be found in the report of the *n_TOF* collaboration.

2 Finalization of the new GEM detector with remote electronics

As outlined in the previous report, the main objective was to realize a new GEM detector with remote front-end electronics and evaluate the capability of the used micro-coaxial cables to transport signals in terms of noise and charge. In fact, the new front-end electronics has been realized

with a PCB pad board (fig. 1a) and 64D GEMINI cards [1] equipped with special connectors to insert micro-coaxial cable between them (fig. 1b). These components have also been realized by the Nuclear Instrument company, which provided cables of different lengths, from a minimum of 5 cm to a maximum of 2 m (fig. 1c).

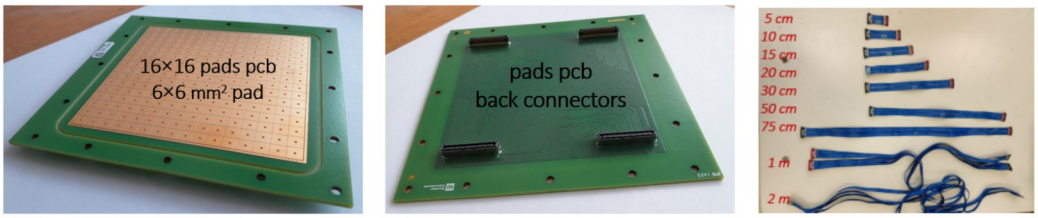

(a) (b) (c)

Figure 1: *a) 16×16 pads PCB board; b) the back side of the PCB board; c) set of micro-coaxial cables with different lengths.*

These tests have been performed by inducing electronic signals on the PCB pads similar to those induced by X-rays and using cables of different lengths. As a result, it has been demonstrated that the remote control of read-out electronics can be realized by obtaining a satisfying signal transport with cables at least 1 m long. The next step was the realization of the new triple-GEM chamber (fig. 2): similarly to the standard configuration used for our 10×10 cm^2 GEM detectors [2], the new chamber was composed of three GEM foils with gap of 1, 2 and 1 mm between them and the pads PCB. The active region between the cathode and the first GEM foil was realized with a gap of 6 mm to increase its efficiency.

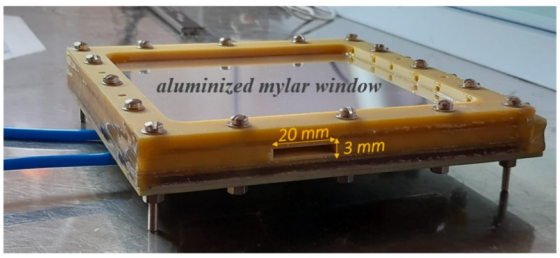

Figure 2: *A photo of the new assembled GEM detector that shows the main head-on mylar window (100×100 mm^2) and one side-on window (3×20 mm^2).*

Like the other standard detectors, the cathode is made with an aluminized mylar foil with a thickness of 15 μm, while, unlike the other standard detectors, the first two GEM foils from the active region have been realized in Aluminum. This choice arises from the experimental observation that the fluorescence line at 8 keV from copper of standard GEM foils introduces a parasitic peak in the spectral range that the detector must investigate as diagnostic system on modern fusion reactors. On the contrary, Aluminum has a fluorescent line at about 1.5 keV, but its effect can be easily removed with gain and threshold working parameters. The pads PCB anode has been fixed with an O-ring system so that it could be replaced with other PCB anodes. In addition, the chamber has been equipped with two side windows of 20×3 mm^2 that can be useful for the

detection of hard X-rays in side-on configuration. Before mounting the PCB anode, pads matrix has been mapped in order to have the correct channel correspondence with acquisition software. Then, the new chamber with its readout electronics and 1 m long micro-coaxial cables has been tested by using a ^{55}Fe source (fig. 3).

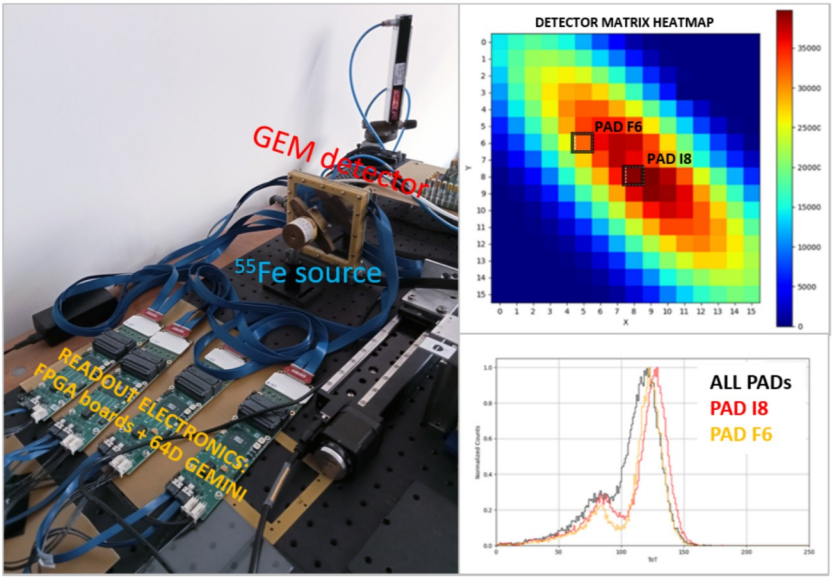

Figure 3: *On the left: a photo of the experimental set-up in the NIXT lab showing the main elements; on the right: the cumulative ToT image of the X-ray emission from the* ^{55}Fe *source and the ToT spectra for all pads and the two marked pads.*

The used gas mixture was $ArCO_2$ (70/30) at atmospheric pressure. A first analysis of the results coming from these tests allowed to evaluate that optimal gain voltage with aluminized GEM foils is about 20 V higher per GEM with respect to the standard copper-plated GEM foils. In particular, a scan with different gain voltages provided a range of optimal values where the ToT spectra can be measured with the best energy resolution of less than 20% (fig. 4).

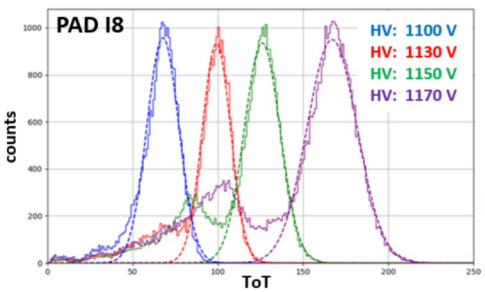

HV (V)	Mean	FWHM
1100	67.7	22.1
1130	99.2	19.6
1150	126.0	24.8
1170	167.0	36.6

BEST ENERGY RESOLUTION ≤ 20 %

Figure 4: *ToT spectra for the most intense pad obtained at different gain voltages with the relative gaussian fit that provides the mean value and the FWHM. The best energy resolution is obtained in the range between 1130 and 1150 V.*

As observed, aluminized GEM foils work with different gain voltages and then an energy calibration will be necessary to finalize the detector characterization. To this purpose, recently, experimental tests have been performed by using the characteristic fluorescent lines from different materials (Ti, Fe, Cu, Pb and Mo). At the moment, acquired data are under analysis and results will be ready in the first months of the current year.

3 Side-on GEM detector for hard X-rays measurements

The new GEM detector in a side-on configuration arises from the need to make charge measurements on the X emission from laser plasma (fig. 5). Typically, X-ray emission from these sources lasts for few tens on ps and X-ray photons cannot be measured separately. With this detector, the idea is to measure absorption profiles to estimate the incident spectrum. It has an active region with a gap of 12 mm with 6×80 mm^2 side-on windows. The pads PCB is divided in 4 rows with 64 pads, each with an area of 1.5×20 mm^2.

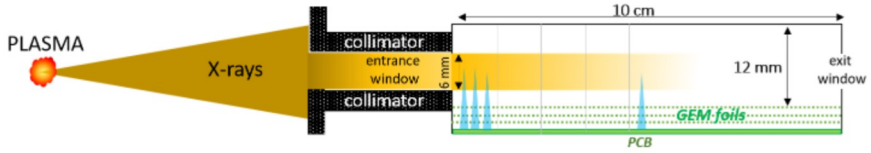

Figure 5: *Layout schema of the side-on triple-GEM detector with 12 mm of active gas layer and* 10×10 *cm*^{2} *area.*

However, in the field of magnetic confinement fusion, it could also be useful the measurement of the hard X-ray spectrum (20 - 60 keV) that arise from some impurities inside the plasma. Then the side-on GEM detector can offer the possibility to realize the hard X-ray spectroscopy because it takes advantage of X-ray absorption on a depth of 10 cm of the gas mixture. First tests with hard X-rays have been performed at the X-ray lab of the CNR Institute for Plasma Science and Technology in Milan. The idea was to realize a set of measurements on some characteristic fluorescent lines from Mo (17.5 and 19.6 keV), Ag (22 keV) and Gd (43 keV) and study the spectral response of the detector. As usual, line emissions have been produced by exciting the material with the X-ray tube (fig. 6).

Figure 6: *Photos of the experimental set-up at the CNR-ISTP X-ray lab in Milan. On the left, the X-ray tube with the target; on the right the installed side-on GEM detector.*

The fluorescence spectrum has been measured with a Si-PIN spectrometer in the position of the GEM detector, in order to evaluate the presence of other parasitic contributions and try to minimize them. As a result, it has been observed that the extraction of the Gd line was not optimal due to the presence of other line emissions at lower energies coming especially from the tungsten anode of the X-ray tube. In addition, the active gas mixture used for the GEM detector was $ArCO_2$ (70/30) and the efficiency is less than 1%. However, measurements have been performed for all the three materials with a scan in threshold and in gain. Some preliminary results of the measured profiles in ToT coming from Mo and Ag targets are summarized in fig. 7.

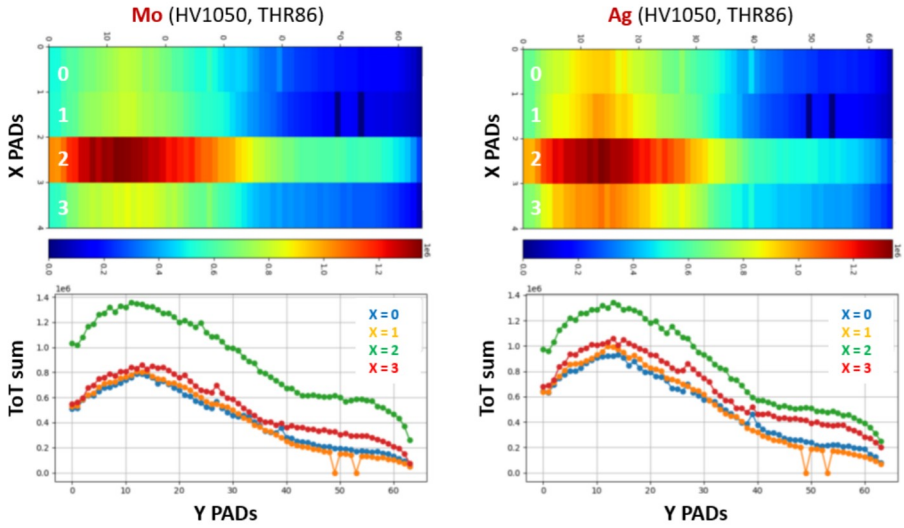

Figure 7: *Measured absorption profiles for Mo and Ag target as obtained in 2D and reconstructed in 1D line by line on the 64 pads.*

Interaction of higher energy photon produces a more significant charge sharing effect and then a dedicated algorithm has been developed to cluster the pads activated by a single photon. In fig. 8, some preliminary results of this analysis are outlined and ToT distributions have been realized by selecting the different observed cluster sizes.

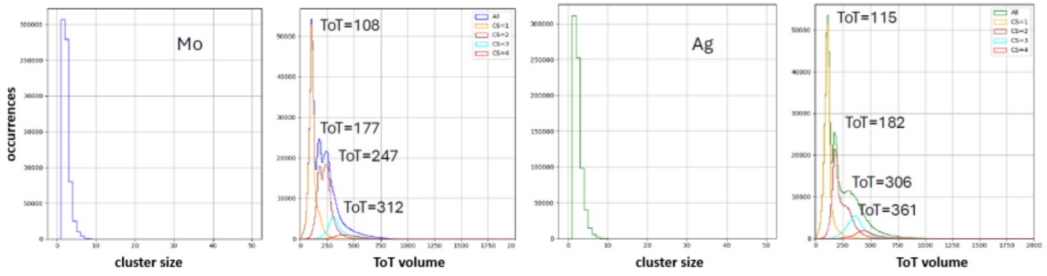

Figure 8: *Histograms of cluster size and ToT volume for Mo and Ag targets. ToT volume histograms have been separated according to the different observed cluster sizes.*

As can be observed, the main ToT peak results from single cluster size events, while double cluster size events give rise to secondary peaks that probably can be associated to the characteristic emission lines of the materials. The main peak, instead, derives from the low energetic lines due to the tungsten anode of the X-ray tube. Peaks corresponding to larger cluster size could be associated to the higher energy background. At the moment, however, all these results are under analysis and their interpretation must be confirmed.

4 X-rays profile measurements in LPP experiments with the side-on GEM

First measurements of the X-rays emission from a laser plasma have been performed on the laser facility at the CNR-INO research center in 2022. The used laser was a Ti:Sa CPA (Chirped Pulse Amplification) that can reach a power of 240 TW and a pulse duration of a few tens of fs. The side-on GEM detector was installed out in air in front of a port placed on the same side of the incident laser and the material targets used during the first campaign were thin sheets of Ti, Al, Cu, and Mylar. For more information, the reader can refer to previous years' reports. Based on the obtained results, a set of critical issues have been highlighted, in particular, the EMP has not been fully shielded and continues to produce random noise that adds to the physical signal, and the charge detected on the first entrance pads can saturate the preamplifier resulting in an incorrect reconstruction of the absorption profiles. To minimize these effects, a new pads PCB layout has been designed with the aim to realize a new side-on GEM prototype. The new pad layout has been conceived again as 4 rows with 64 pads but with a shorter length and a variable width from 1 to 2.5 mm (fig. 9).

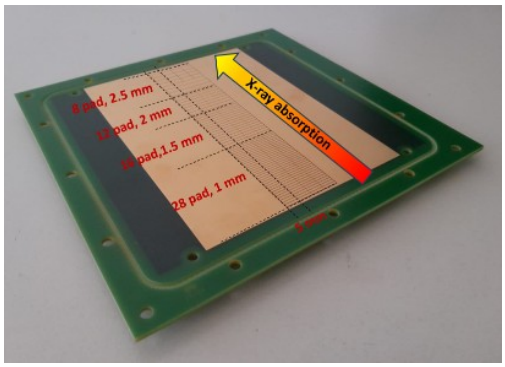

Figure 9: *A photo of the new pads PCB realized having 4 rows with 64 pads at varying width.*

Due to smaller pad areas, it is expected a reduction of the induced EMP noise and a lower charge on a single pad that, together with the charge sharing effect, will avoid the single channel saturation. In addition, this new pads PCB is equipped with Samtec cable connectors and then like the head-on GEM described in paragraph 2, its readout electronics can be carried out remotely. This could represent a further advantage to minimize the EMP disturbances that often affects the complex electronic readout systems.

5 Timepix3-based neutron diagnostic for LPP experiments

Between late May and early June 2024, our group had the opportunity to participate in a laser plasma experiment at the ELI Beamlines facility (Prague, Czech Republic) to perform measurements of medium-energy neutrons at 2.45 MeV produced by the interaction of a high-power laser on a deuterated plastic target. In this experiment, in addition to the neutron Diamondpix [3; 4] and the 1 mm Si Timepix3 [5; 6], a Timepix3 quad detector with 100 μm thick silicon [7; 8] and equipped with a 100 μm polyethylene converter placed 1 mm from the detector surface was used (fig. 10).

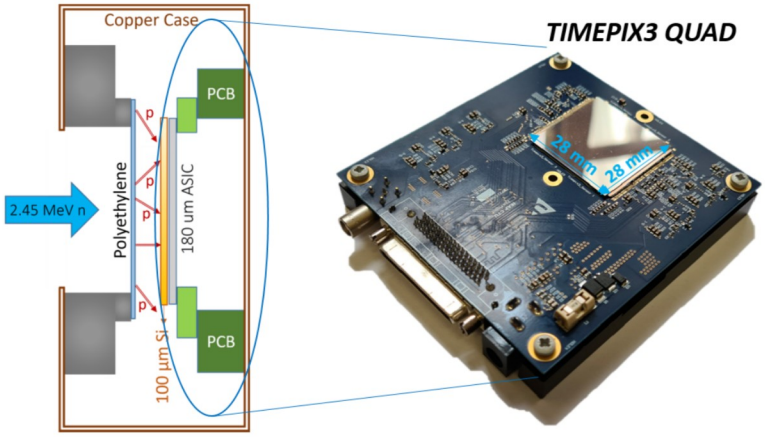

Figure 10: *A schema of the fast neutron system based on a Timepix3 quad combined to a polyethylene foil with a thickness of 100 μm.*

For these measurements the quad has been placed at a distance of about 130 cm and it was also possible to exploit the time-of-flight measurements to identify neutrons. It was also necessary to shield the intense flash gamma produced when the laser interacted with the target with 5 cm thick lead blocks (fig. 11).

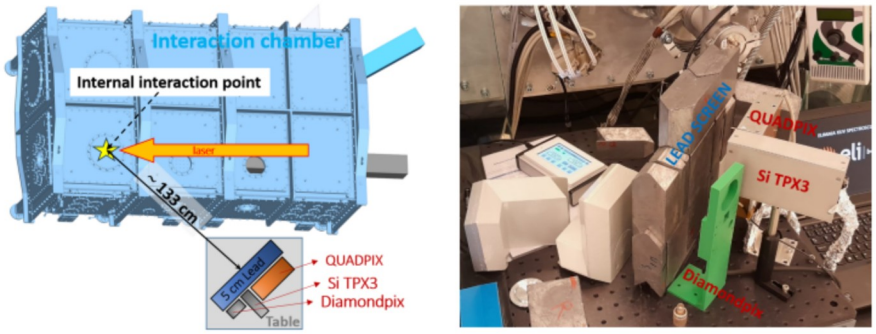

Figure 11: *On the left: a schema of the experimental set-up on the ELI facility showing the interaction chamber and the position of the three detectors respect to the interaction point; on the right: a photo of the three installed detectors with the lead screen before.*

At a distance of about 130 cm from the interaction point the expected number of neutrons reduced drastically. However, a comparison of Time of Flight measurements between the non-deuterated and deuterated targets shows a delayed peak at about 80 ns with respect to the main gamma flash peak (fig. 12).

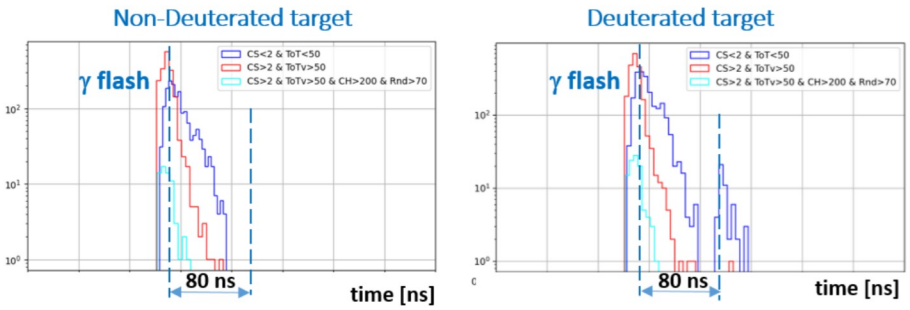

Figure 12: *Three histogram distribution of the ToF time as obtained by applying different cuts on the cluster parameters for a non-deuterated and a deuterated plastic target. The blue one shows a 80 ns delayed peak with deuterated target that corresponds to neutron of about 2.4 MeV.*

This result could be a confirmation of the expected 2.45 MeV neutrons coming from the DD reaction induced by the laser. A further test at the FNG facility with an AmBe neutron source demonstrated that the few identified tracks with ToF measurements fall in the recoil proton region as observed by combining cluster size and ToT volume track parameters. The other two detectors, the 1 mm Si Timepix3 and Diamondpix have been placed to detect gamma photons and neutrons, respectively. While the first provided some indications on the photon flux, the second revealed an insufficient number of events to confirm the presence of neutrons.

6 Analytical Modeling of a Proton Recoil Telescope for Neutron Spectrometry

A general analytical model for the response function of a Proton Recoil Telescope (PRT) has been developed, building on the foundational work of Weise (1968). In fusion diagnostics, precise neutron spectrometry is essential since D-D fusion produces 2.45 MeV neutrons and D-T fusion produces 14.1 MeV neutrons. Proton Recoil Telescopes offer excellent energy resolution (ΔE/E $\sim$ 2–5%) over a wide energy range (1–30 MeV) with directional sensitivity. The core challenge lies in accurately computing the response function n(E, E'), which enters a Fredholm integral equation of the first kind — a notoriously ill-conditioned inverse problem — relating the measured proton spectrum to the unknown neutron spectrum.

In the PRT setup, a neutron of energy E_n strikes a hydrogen nucleus in a polyethylene converter foil. A proton is ejected with initial energy $E_{p1} = E_n cos^2\theta$, then loses energy as it traverses the foil, and is finally detected with energy E_p by a silicon detector. The response function's shape depends critically on the geometry (source, converter, detector) and on the converter thickness. Our generalized analytical formulation separates the response function into three contributions: physics constants (the n-p elastic scattering cross section, nearly isotropic in the center-of-mass

frame up to ∼10 MeV), the energy loss factor (described via the Bragg–Kleeman range-energy relation), and a geometric factor that encodes the full complexity of the experimental setup.

For the specific case of on-axis cylindrical geometry with a parallel neutron beam, a rigorous derivation of the geometric factor f(θ) has been carried out, recovering the well-established results of Gotoh (1973) as a limiting case. Furthermore, two simplified asymptotic formulas have been derived for the equal-radius configuration ($r_1 = r_2 =$ r): one for $d/r < 1$ (close geometry) and one for $d/r > 1$ (far geometry), where d is the converter-to-detector distance. These asymptotic expressions enable rapid evaluation of the response function without numerical integration of the full geometric factor, greatly facilitating experimental design and system optimization.

The analytical model has been rigorously validated against Geant4 Monte Carlo simulations. A detailed simulation setup was constructed with a 13×13 cell array ($14.3 \times 14.3\ mm^2$) including a polyethylene converter of variable thickness, a 2.5 mm stainless steel collimator with 1.0 mm diameter holes, a 100 nm Mylar window, and a 300 μm thick silicon detector. Simulations were run with 6.0×10^9 primary 2.45 MeV neutrons for polyethylene thicknesses of 5, 15, 30, 50, and 100 μm. The model accurately reproduces the characteristic "shark fin" shape of the response function: a sharp cutoff at the high-energy end from protons generated near the front of the converter (with minimal energy loss), and a broad tail at lower energies from protons originating deeper within the converter. As expected, thicker converters increase detection efficiency but degrade energy resolution by producing broader peaks. The Bragg–Kleeman best-fit parameters for polyethylene ($\alpha = 1.85321 \times 10^{-3}$, a = 1.80173) from NIST data were used in the analytical formula. The comparison across five converter thicknesses shows excellent agreement between the analytical predictions and the Monte Carlo data, demonstrating the model's accuracy and its value as a fast, powerful tool for PRT design and optimization. This work was presented at the 111^{th} SIF Congress in Palermo.

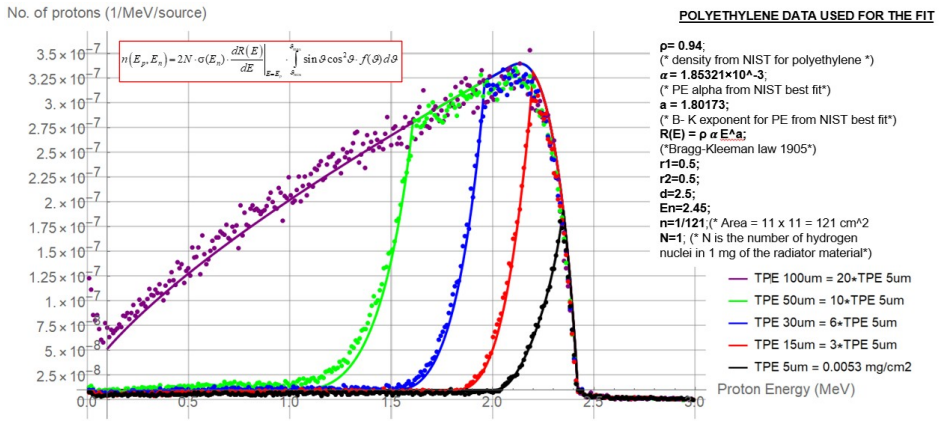

Figure 13: *Comparison between the analytical model (solid lines) and Geant4 Monte Carlo simulations (dots) for the proton recoil spectrum at E_n = 2.45 MeV with five polyethylene converter thicknesses (5, 15, 30, 50, and 100 μm). The inset shows the analytical response function formula used for the fit, and the right panel lists the polyethylene parameters from NIST data.*

7 List of Conference Talks by LNF Authors in Year 2025

1. V. De Leo, Development of a GEM detector prototype with remote front-end electronics system for high-radiation environments, 51^{st} EPS Conference on Plasma Physics, 7 – 11 July 2025 Vilnius, Lithuania

2. D. Pacella, Single and quad silicon Timepix3 detectors to detect neutrons and charged particles in laser plasma experiments, PLASMA 2025 International Conference on research and application of Plasmas, 15-18 September 2025, Warsaw, Poland

3. F. Cordella, Analytical Modeling of a Proton Recoil Telescope (PRT) for Neutron Spectrometry and Fusion Diagnostics, 111° Congresso nazionale della Società Italiana di Fisica, 22 - 26 settembre 2025, Palermo

8 Publications

List of papers published by Frascati INFN_E members in 2025:

1. V. De Leo, G. Claps, F. Cordella, D. Pacella, A. Tamburrino, "Development of a GEM detector prototype with remote front-end electronics system for high-radiation environments", EPS Plasma Physics 2025, P5.286

2. A. Celora, F. Guiotto, F. Caruggi, S. Cancelli, G. Claps, F. Cordella, V. De Leo, L. Garzotti, G. Grosso, E. Lazzaro, D. Pacella, O. Putignano, E. Rose, R. Sarwar, R. Scannell, M. Tardocchi, G. Croci, A. Muraro and the MAST-U. team, Analysis of neutron related background of the SXR GEM diagnostic on MAST-U, Journal of Instrumentation, Volume 20, May 2025

3. A. Celora, F Caruggi, O. Putignano, S. Cancelli, G. Claps, F. Cordella, L. Garzotti, G. Gorini, G. Grosso, F. Guiotto, E. Lazzaro, M. Nocente, D. Pacella, E. Perelli Cippo, D. Rigamonti, E. Rose, R. Sarwar, R. Scannell, F. Scioscioli, M. Tardocchi, G. Croci and A. Muraro, Assessment of a space and energy resolved diagnostic based on GEM technology on MAST-U, Meas. Sci. Technol. 36 (2025) 016019

4. F. Cordella, M. Cappelli, M. Ciotti, G. Claps, V. De Leo, C. Mazzotta, D. Pacella, A. Tamburrino, F. Panza, Genetic algorithm for multilayer shield optimization with a custom parallel computing architecture, Eur. Phys. J. Plus, 2024, doi: 10.1140/epjp/s13360-023-04842-0

References

1 . A. Pezzotta, G. Corradi, G. Croci, M. De Matteis, F. Murtas, G. Gorini, A. Baschirotto, GEMINI: A triple-GEM detector read-out mixed-signal ASIC in 180nm CMOS, in 2015 IEEE International Symposium on Circuits and Systems (ISCAS) (2015), pp. 1718–1721

2 . A. Muraro et al., Development and characterization of a new soft x-ray diagnostic concept for tokamaks, Journal of Instrumentation, Volume 14, Article number C08012 (2019)

3 . A. Tamburrino. Characterization of a new pixelated diamond detector for fast neutron diagnostics on fusion reactors. PhD Thesis at Sapienza University of Rome, Department of Astronautical, Electrical and Energy Engineering, 2024.

4 . G. Claps, F. Murtas, L. Foggetta, C. Di Giulio, J. Alozy, and G. Cavoto, Diamondpix: A CVD diamond detector with timepix3 chip interface. IEEE Transactions on Nuclear Science, 65(10):2743–2753, 2018.

5 . V. De Leo, G. Claps, F. Cordella, G. Cristoforetti, L.A. Gizzi, P. Koester, D. Pacella, A. Tamburrino, "Combined Spectroscopy System Utilizing Gas Electron Multiplier and Timepix3 Technology for Laser Plasma Experiments," Condens. Matter, vol. 8, no. 4, 2023, doi: 10.3390/condmat8040098.

6 . G. Claps et al., Timepix3 detector and Geant4-based simulations for gamma energy detection in Laser Produced Plasmas, JINST, Volume 14, Issue 92 September 2019 Article number P09005

7 . T. Poikela, J. Plosila, T. Westerlund, M. Campbell, M. De Gaspari, X. Llopart, V. Gromov, R. Kluit, M. van Beuzekom, F. Zappon, V. Zivkovic, C. Brezina, K. Desch, Y. Fu, and A. Kruth, Timepix3: a 65k channel hybrid pixel readout chip with simultaneous toa/tot and sparse readout. Journal of Instrumentation, 9, 2014.

8 . P. Burian, P. Broulim, B. Bergmann, M. Farkaš, M. Jára, O. R˚uži˘cka, P. Smolyanskiy, P. Mànek, Katherine generation 2: advanced readout system for timepix3 detectors. JINST (2025). https://doi.org/10.1088/1748-0221/20/06/C06077